The lattice as allosteric effector: Structural studies of $\alpha\beta$- and γ-tubulin clarify the role of GTP in microtubule assembly

Luke M. Rice, Elizabeth A. Montabana, and David A. Agard*

Department of Biochemistry and Biophysics and Howard Hughes Medical Institute, University of California, San Francisco, CA 94158-2517

Contributed by David A. Agard, February 5, 2008 (sent for review December 26, 2007)

GTP-dependent microtubule polymerization dynamics are required for cell division and are accompanied by domain rearrangements in the polymerizing subunit, $\alpha\beta$-tubulin. Two opposing models describe the role of GTP and its relationship to conformational change in $\alpha\beta$-tubulin. The allosteric model posits that unpolymerized $\alpha\beta$-tubulin adopts a more polymerization-competent conformation upon GTP binding. The lattice model posits that conformational changes occur only upon recruitment into the growing lattice. Published data support a lattice model, but are largely indirect and so the allosteric model has prevailed. We present two independent solution probes of the conformation of $\alpha\beta$-tubulin, the 2.3 Å crystal structure of γ-tubulin bound to GDP, and kinetic simulations to interpret the functional consequences of the structural data. These results (with our previous γ-tubulin:GTPγS structure) support the lattice model by demonstrating that major domain rearrangements do not occur in eukaryotic tubulins in response to GTP binding, and that the unpolymerized conformation of $\alpha\beta$-tubulin differs significantly from the polymerized one. Thus, geometric constraints of lateral self-assembly must drive $\alpha\beta$-tubulin conformational changes, whereas GTP plays a secondary role to tune the strength of longitudinal contacts within the microtubule lattice. $\alpha\beta$-Tubulin behaves like a bent spring, resisting straightening until forced to do so by GTP-mediated interactions with the growing microtubule. Kinetic simulations demonstrate that resistance to straightening opposes microtubule initiation by specifically destabilizing early assembly intermediates that are especially sensitive to the strength of lateral interactions. These data provide new insights into the molecular origins of dynamic microtubule behavior.

dynamic instability | microtubules

Microtubules are hollow cylindrical polymers of $\alpha\beta$-tubulin that are critical for intracellular trafficking and formation of the mitotic spindle required for chromosome segregation during cell division. Although vitally important, the molecular mechanisms underlying dynamic microtubule (MT) behavior are poorly understood. Microtubule assembly requires GTP-bound $\alpha\beta$-tubulin, and GTP hydrolysis by β-tubulin is required to generate dynamic MTs (reviewed in ref. 1). Structural studies have demonstrated two extreme conformations of $\alpha\beta$-tubulin: a "straight" conformation observed in the MT lattice (2), and a "curved" conformation observed in a structure of $\alpha\beta$-tubulin complexed with colchicine and a stathmin-like domain (3) (Fig. 1). There are two opposing models for the relationship between GTP and conformational change in $\alpha\beta$-tubulin. The allosteric model (recently reviewed in ref. 4) postulates that GTP binding to $\alpha\beta$-tubulin triggers long-range conformational changes yielding a substantially straighter conformation that is prestructured in solution for lateral interactions (5). The lattice model (6) postulates that in solution, $\alpha\beta$-tubulin adopts the MT-incompatible, curved conformation independent of nucleotide state. Thus, the conformational changes accompanying straightening are the consequence, not the cause, of lattice assembly. The role of GTP is to tune the strength of the MT lattice contacts (Fig. 1) either directly (the γ-phosphate interacting with conserved residues in the α-tubulin T7 loop), or indirectly (the γ-phosphate directing local restructuring of proximal β-tubulin residues to interact more optimally with α-tubulin). The controversy remains unresolved in large part because most of the evidence for either model is indirect. Here we present results that argue strongly in favor of the lattice model. We then use kinetic simulations to show that the lattice model predicts a selective destabilization of critical nucleation intermediates, exaggerating the difficulty of *de novo* polymer initiation.

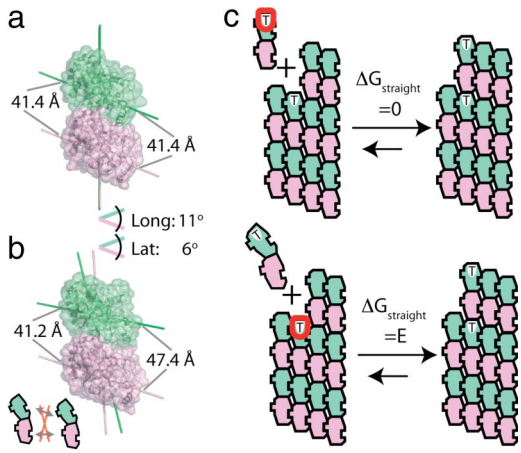

Fig. 1. Two conformations of $\alpha\beta$-tubulin, and conflicting models for the role of GTP. (*a*) Longitudinal and lateral interaction surfaces are aligned in the straight (1JFF, top), but not in the curved (1SA0, bottom) conformation. In the curved conformation, the α- and β-tubulin protofilament and lateral interaction axes are skewed by 11° and 6°, respectively; these rearrangements separate equivalent laterally interacting atoms by up to 6 Å. (*Inset*) This misalignment of interfaces destabilizes lateral interactions between curved $\alpha\beta$-tubulins. (*b*) In the allosteric model, GTP (circled in red) stimulates MT assembly by inducing the straight, MT-compatible conformation in unpolymerized $\alpha\beta$-tubulin. Incorporation into the lattice is not associated with unfavorable domain rearrangements ($\Delta G_{straight} = 0$). (*c*) In the lattice model, unpolymerized $\alpha\beta$-tubulin remains curved even when bound to GTP. Incorporation into the lattice requires unfavorable domain rearrangements ($\Delta G_{straight} = E$). The lattice-acting GTP (circled in red) provides stronger lattice contacts to stabilize the MT-bound straight conformation.

Author contributions: L.M.R. designed research; L.M.R. and E.A.M. performed research; E.A.M. contributed new reagents/analytic tools; L.M.R. and D.A.A. analyzed data; and L.M.R. and D.A.A. wrote the paper.

The authors declare no conflict of interest.

Freely available online through the PNAS open access option.

Data deposition: The atomic coordinates and structure factors have been deposited in the Protein Data Bank, www.pdb.org (PDB ID code 3CB2).

*To whom correspondence should be addressed. E-mail: agard@msg.ucsf.edu.

This article contains supporting information online at www.pnas.org/cgi/content/full/0801637105/DCSupplemental.

© 2008 by The National Academy of Sciences of the USA

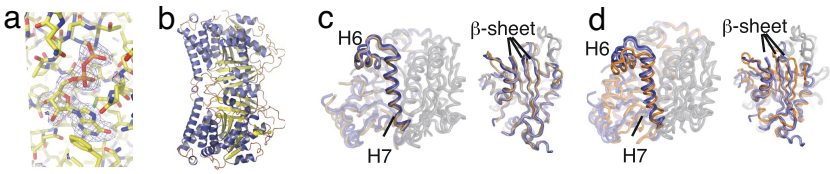

Fig. 2. Structural features of γ-tubulin:GDP. (*a*) $F_o - F_c$ electron density computed from the final model with GDP omitted. The nucleotide binding site of chain A is shown. (*b*) The twofold noncrystallographic symmetry interaction between γ-tubulins (Chain A, dark blue and yellow; Chain B, light blue and pale yellow). The nucleotide binding sites (''plus'' ends) are top and bottom. (*c*) γ-Tubulin:GDP (chain A, dark blue; chain B, light blue) and γ-tubulin:GTPγS (tan) adopt the same curved domain organization. See also Table S2. (*Left*) Helices H6 and H7. (*Right*) The intermediate domain β-sheet (helix H10, which would obscure the view of the β-sheet, has been omitted for clarity). (*d*) γ-tubulin:GDP (colors as in *c*) shows characteristic differences when compared with the straight conformation of β-tubulin (PDB code: 1JFF, orange). *Left* and *Right* are as in *c*.

Because it has not been possible to determine the atomic structure of αβ-tubulin:GTP, the allosteric model is largely based on electron microscopic observations (e.g., ref. 7) that showed straight (or, more recently, straighter; refs. 5 and 8) protofilaments in MTs grown from GTP-bound αβ-tubulin but showed curved assemblies in samples of GDP-bound αβ-tubulin. Importantly, these data generally derive from large, multiprotofilament assemblies of αβ-tubulin (5, 9).

Crystallographic studies of αβ-tubulin and related proteins (3, 10–13) have begun to challenge the allosteric model. The crystal structure of αβ-tubulin bound to colchicine and a stathmin-like domain provided the first atomic model for the curved conformation (3), revealing that curvature at the heterodimer level was generated by similar domain rearrangements in both α- and β-tubulin subunits, despite GTP being bound to the α-subunit. Our recently reported crystal structure of γ-tubulin:GTP (10) unexpectedly adopted this curved domain arrangement. Multiple crystal structures of more distantly related monomeric bacterial tubulin homologs also showed a curved domain arrangement independent of the nucleotide bound (12, 14, 15) (reviewed in ref. 4).

Solution experiments have also provided data arguing against nucleotide-dependent conformational changes in unassembled αβ-tubulin. Colchicine-type ligands destabilize MTs by binding to a pocket in αβ-tubulin that is only accessible in the curved, unpolymerized conformation (3). Thus, if straight and curved conformations result from GTP- and GDP-binding, then differences in the affinity of αβ-tubulin for colchicines should be observed. No such differences have been detected (17). More directly, small-angle x-ray scattering (SAXS), which should be sensitive to differences in domain arrangement, failed to detect nucleotide-dependent conformational changes (18).

Unfortunately, the existing evidence is not yet sufficient to unambiguously define which model is correct. The solution data for unpolymerized αβ-tubulin (SAXS and allocolchicine binding) were for technical reasons performed in the absence of Mg^{2+} known to be critical for proper high-affinity GTP binding. They may therefore have failed to populate the fully active αβ-tubulin:GTP:Mg^{2+} complex. The bacterial tubulin homologs do not form MTs (19), and in fact do not make MT-like lateral associations at all (13, 20). Therefore, they may not provide a reliable model for any potential linkage between nucleotide state and conformational change required by eukaryotic tubulins to form the lateral associations necessary for MT assembly. Finally, without an accompanying GDP-bound structure, it is impossible to assert with confidence that domain rearrangements do not accompany GTP-binding by γ-tubulin.

In this work, we sought to better resolve the nature of potential nucleotide-dependent conformational changes in eukaryotic tubulins by directly studying eukaryotic tubulins. We determined the atomic structure of human γ-tubulin:GDP, and thereby provide the only GTP/GDP pair of eukaryotic tubulin structures. We also used two independent methods, allocolchicine binding and SAXS, this time in the presence of Mg^{2+}, to directly probe the solution conformation of unpolymerized αβ-tubulin as a function of bound nucleotide. Our results contribute to the rising tide of evidence that, in both γ- and αβ-tubulin, domain rearrangements do not occur in response to GTP binding. They argue strongly for the lattice model, in which the GTP acts indirectly to tune to strength of polymerization contacts. Exploring the potential consequences of this change in perspective with kinetic models reveals that the lattice model predicts unanticipated barriers affecting MT initiation intermediates.

Results

γ-Tubulin:GDP Adopts a Curved Conformation Identical to That of γ-Tubulin:GTPγS. γ-Tubulin crystallizes more readily than αβ-tubulin, allowing us to obtain a new crystal form of γ-tubulin bound to GDP [supporting information (SI) Table S1 and Fig. 2*a*]. These better diffracting crystals (2.3 Å) contain two γ-tubulins in the asymmetric unit (Fig. 2*b*). The improved resolution allowed us to identify a chain tracing error in our recent GTPγS (guanosine 5'-[γ-thio]triphosphate) structure (10), extending the loop between helices H11 and H12 and shifting the register of the C-terminal helix by three residues (Fig. S1). The local structure of the nucleotide binding site and the overall conformation of γ-tubulin:GDP and γ-tubulin:GTPγS are strikingly similar (overall C_α rmsd 0.78 Å and 0.63 Å for chain A and chain B, respectively) (Fig. 2*c*). The domain arrangement in the γ-tubulin:GDP structures closely resemble those seen in the γ-tubulin:GTPγS structure (10) and in the curved αβ-tubulin crystal structures (Fig. 2*c*) (3, 11).

Lateral Interactions Between γ-Tubulins Are Adaptable and Are Not Regulated by Nucleotide. A key difference between the bacterial and eukaryotic tubulins is the ability to form MT-like lateral interactions. Lateral interactions similar to those that we observed in the γ-tubulin:GTPγS crystal (10) are again present in the γ-tubulin:GDP crystals despite different crystal packing (Fig. S2). This indicates that MT-like lateral interactions between γ-tubulin monomers can occur independent of nucleotide state (Fig. S2).

Our γ-tubulin structures clearly indicate that γ-tubulin does not undergo curved-straight domain rearrangements in response to its nucleotide state. This lack of nucleotide-linked domain rearrangements in momomeric tubulins is consistent with the behavior of prokaryotic tubulin homologs (12–15), and distinguishes this family of proteins from signaling GTPases that are known to switch conformation in response to nucleotide state. This distinction likely arises because the tubulin fold is quite different from that of the switching GTPases, lacking cognates of the P-loop and switch regions that respond to nucleotide state (21, 22). To rule out the possibility that these monomeric tubulins behave differently from heterodimeric αβ-tubulin, we sought methods capable of reporting on the solution conformation of αβ-tubulin in the absence of any higher-order self-assembly.

BIOPHYSICS

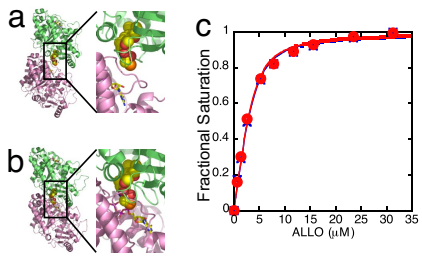

Fig. 3. The affinity of $\alpha\beta$-tubulin for allocolchicine does not depend on nucleotide state. (*a*) The colchicine binding pocket as observed in the crystal structure of the curved conformation (1SA0, ref. 3). Colchicine (spheres) binds between α- (pink) and β-tubulin (green), near the nonexchangeable GTP (sticks). (*b*) Colchicine binding is not compatible with the straight conformation of $\alpha\beta$-tubulin. Modeling colchicine into the straight conformation of $\alpha\beta$-tubulin reveals steric clashes with atoms α- and β-tubulin and the nonexchangeable GTP. (*c*) Saturation binding curves of allocolchicine binding to $\alpha\beta$-tubulin in the presence of 1 mM GTP (blue, crosses) or 1 mM GDP (red, squares). Dissociation constants obtained by fitting the curves (solid lines) are 0.79 $\pm$ 0.15 μM and 0.74 $\pm$ 0.15 μM for $\alpha\beta$-tubulin:GTP and $\alpha\beta$-tubulin:GDP, respectively.

Allocolchicine Binding Is Conformation-Dependent, but Allocolchicine Affinity Is Independent of Nucleotide State. Colchicine-type drugs are MT depolymerizers that bind in an open cleft between α- and β-tubulin that becomes substantially occluded in the straight conformation (3) (Fig. 3 *a* and *b*). If GTP binding to β-tubulin were to alter the balance between straight and curved $\alpha\beta$-tubulin conformations, measurable nucleotide-dependent differences in the colchicine binding affinity should result. We used allocolchicine, a well characterized colchicine analog (23, 24), to address this question. Allocolchicine fluoresces only when bound to $\alpha\beta$-tubulin Fig. S3. A study performed before the $\alpha\beta$-tubulin:colchicine structure was determined had attempted to identify the colchicine binding site by examining the effect of allocolchicine binding on the dissociation of $\alpha\beta$-tubulin into subunits (17). This work indicated that allocolchicine binds $\alpha\beta$-tubulin with identical affinity when either GTP or GDP is bound, but unfortunately Mg^{2+} was omitted because it affected the dissociation of $\alpha\beta$-tubulin into subunits and therefore represented a confounding factor (25). To eliminate the possibility that omitting Mg^{2+} resulted in an artificial failure to observe a nucleotide-dependent change in affinity, we performed similar experiments with Mg^{2+} present. The slow GTPase rate of colchicine-bound $\alpha\beta$-tubulin (26) and the ease of GDP exchange (27, 28) combine to make measurements with GTP possible. Equilibrium binding curves for $\alpha\beta$-tubulin:allocolchicine binding in the presence of 1 mM GTP or 1 mM GDP and 1 mM Mg^{2+} are shown in Fig. 3c. The measured affinity of $\alpha\beta$-tubulin for allocolchicine (GTP: 0.79 $\pm$ 0.15 μM, GDP: 0.74 $\pm$ 0.15 μM) is independent of the nucleotide bound to $\alpha\beta$-tubulin. Thus, any nucleotide-dependent conformational changes that might occur in $\alpha\beta$-tubulin cannot involve domain rearrangements that would significantly alter the curvature of the heterodimer. To better specify the actual solution conformation of unpolymerized $\alpha\beta$-tubulin, we turned to solution x-ray scattering.

SAXS Profiles for $\alpha\beta$-Tubulin:GTP and $\alpha\beta$-Tubulin:GDP Are Essentially Identical and Indicative of the Curved Conformation. SAXS provides a sensitive probe of the solution conformation, and has recently been used to answer questions about conformation and conformational change in other molecular systems (29–31). We predicted SAXS intensity profiles using structures representative of curved (3) and straight (2) conformations of $\alpha\beta$-tubulin (Fig. 4*a*). There is a significant fraction ($\approx$6%) of missing atoms in the $\alpha\beta$-tubulin models used to generate the calculated data (see *Methods*), so we also calculated a SAXS profile from a more complete model for the curved conformation that has the γ-tubulin structure in place of α- and β-tubulin (see *Methods*). These predictions show small but significant differences over a large part of the experimentally accessible scattering range (Fig. 4a). By working at relatively low $\alpha\beta$-tubulin concentrations and by using buffer and temperature conditions that do not promote assembly, we were able to measure SAXS profiles for GTP- or GDP-bound $\alpha\beta$-tubulin in the presence of 1 mM $MgCl_2$ (Fig. 4*a*). Our results confirm and extend the earlier studies performed in the absence of Mg^{2+} (18). The intensity profiles and their associated pair distance probability functions [$P(r)$] (Fig. 4*b*) reveal that $\alpha\beta$-tubulin does not undergo detectable curved–straight domain rearrangements in response to nucleotide. Direct fitting of the SAXS intensity curves indicates that our data are best modeled by the most complete heterodimer in a curved conformation (purple curve, Fig. 4*c*), closely followed by the curved $\alpha\beta$-tubulin conformation. Our SAXS analysis, the allocolchicine affinity, and the predominance of the curved conformation in all structures of monomeric tubulins or bacterial homologs (10, 12–15) together strongly argue for the lattice model, in which a curved conformation of the $\alpha\beta$-tubulin heterodimer dominates independent of the nucleotide bound to β-tubulin.

Discussion

$\alpha\beta$-Tubulin has a unique structural property compared with monomeric tubulins: curvature at the monomer level is amplified within the heterodimer. The coupling of quaternary organization to otherwise unfavorable structural transitions within each monomer implies that the $\alpha\beta$-tubulin heterodimer essentially

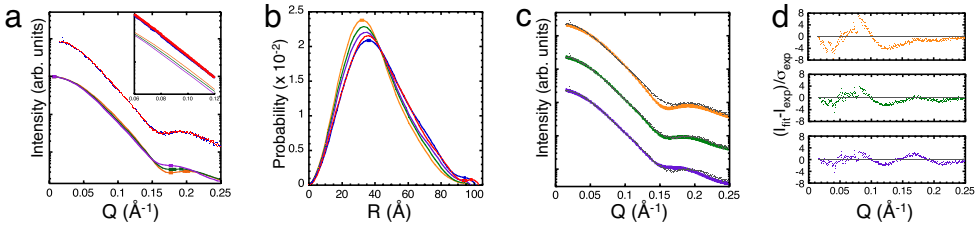

Fig. 4. Small angle x-ray scattering shows that $\alpha\beta$-tubulin:GTP and $\alpha\beta$-tubulin:GDP adopt essentially identical curved conformations. (*a*) Predicted scattering curves for straight (PDB 1JFF, brown), curved (PDB 1SA0, green), and more complete curved (γ-tubulin based model, purple) conformations of $\alpha\beta$-tubulin show differences over most of the scattering range. Measured scattering curves in the presence of 1 mM GTP (blue) or 1 mM GDP (red) are substantially identical. Predicted and measured curves are offset to facilitate comparison. (*Inset*) Same comparison (with less offset between measured and calculated curves) over a narrower Q ($= 4\pi\sin\theta/\lambda$) range where differences between the calculated curves are most apparent. (*b*) Pair–distance probability distributions (colors as in *a*) obtained from the calculated and measured curves in *a*. (*c*) Structural models fit to the $\alpha\beta$-tubulin:GTP SAXS data (gray dots). Straight conformation (1JFF; brown: $\chi^2 = 2.34$), curved conformation (1SA0; green: $\chi^2 = 1.30$), and a more complete model for the curved conformation (purple: $\chi^2 = 1.11$). Fits are offset to facilitate comparison. (*d*) Error-normalized residuals $(I_{calc} - I_{exp})/\sigma_{exp}$ from the fits (same color scheme).

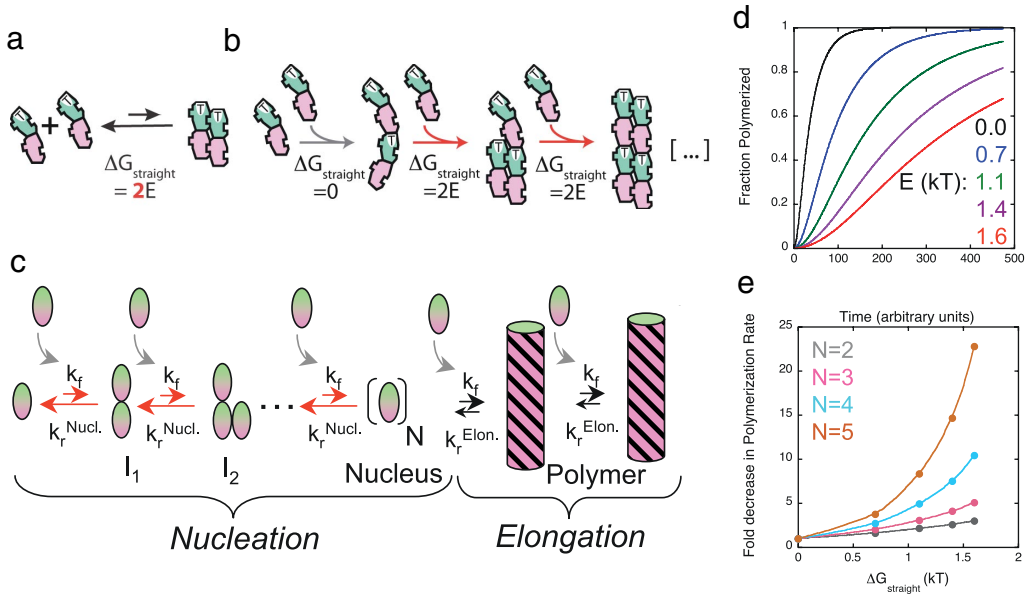

Fig. 5. Implications for the kinetics of MT initiation. (*a*) Assembly-dependent conformational change during MT initiation opposes lateral assembly. In the absence of a straight MT lattice, both $\alpha\beta$-tubulins must change conformation for lateral association. For full straightening, the energetic penalty arising from conformational change during initiation ($\Delta G_{straight} = 2E$) will be double that during elongation. (*b*) Representation of a possible sequence of early MT initiation intermediates, starting from curved $\alpha\beta$-tubulin. Pure longitudinal associations (gray arrows) do not require conformational change. To form lateral associations, however, will frequently require that two $\alpha\beta$-tubulins change conformation (red arrows). These initiation-specific events incur additional energetic costs compared with elongation, and will be selectively disadvantaged (see Fig. 5*c*). (*c*) Representation summarizing the kinetic models (see *Methods*) used to investigate potential consequences of the lattice model. Nucleation is modeled as an arbitrary number of consecutive bimolecular reactions governed by identical association (k_f) and dissociation (k_r^{Nucl}) rate constants. Red arrows indicate steps that incur the energetic cost of straightening. Once a critical oligomer is formed (the nucleus, N subunits), elongation by monomer addition becomes energetically favorable and is governed by the same association rate constant (k_f) and a different dissociation rate constant (k_r^{Elon}). The model treats plus and minus ends of the MT as kinetically indistinguishable (Fig. S4 presents a possible structural explanation of these known kinetic differences). (*d*) Energetically unfavorable assembly-dependent conformational changes decrease the stability of nucleation intermediates. The black curve corresponds to self-association of rigid subunits (no conformational change). The energetic cost of assembly-dependent conformational change ($\Delta G_{straight}$) was estimated at 0.7 (blue), 1.1 (green), 1.4 (purple), and 1.6 (red) *kT*. This corresponds to 2-, 3-, 4-, or 5-fold reductions in the apparent affinity of subunit associations and significantly decreases the apparent rate of MT assembly. (*e*) There is a multiplicative slowing effect when multiple nucleation intermediates require energetically unfavorable assembly-dependent conformational change. The cost of assembly-dependent conformational change as described in *c* was compared by examining the initial polymerization rate among generic nucleation-elongation models identical except for the size of the nucleus (2, gray; 3, pink; 4, cyan; 5, orange; see *Methods*).

behaves like a bent spring, resisting the straightening required to align lateral interaction surfaces (Fig. 1). The lattice model argues that GTP acts *in trans*, strengthening longitudinal interactions and thereby providing sufficient binding energy to recruit and straighten (via lateral interactions) the unpolymerized, curved $\alpha\beta$-tubulin heterodimer (Figs. 1 and 5 and Fig. S4). GDP-mediated longitudinal contacts are presumably too weak to overcome the energetic barrier required to straighten the curved, unpolymerized heterodimer. The default, curved conformation of $\alpha\beta$-tubulin also means that the GTP so critical for assembly is presented in different structural contexts for addition at opposite ends of the microtubule (Fig. S4). The intrinsic asymmetry of the curved conformation thus provides a structural rationale that begins to answer a longstanding question: why do microtubule plus and minus ends show different dynamic behavior and growth kinetics despite having identical affinities for unpolymerized subunits (32).

By specifying that the unpolymerized conformation of $\alpha\beta$-tubulin differs significantly from the polymerized one, the lattice model implies that the MT lattice itself, and not the nucleotide, is the allosteric effector. The lattice model predicts that, because a prestraightened MT lattice does not exist during initiation, lateral interactions will be selectively disadvantaged. Indeed, during an elongation step only one $\alpha\beta$-tubulin must straighten, but to establish a new MT lattice one or more associations in which two $\alpha\beta$-tubulin heterodimers must simultaneously straighten to permit lateral association (Fig. 5*a*).

We performed kinetic simulations to explore the functional consequences of these conformational changes for MT initiation. MT assembly displays hallmarks (prolonged lag phase preceding rapid assembly) typical of so-called nucleation-elongation kinetic mechanisms (33), wherein the rate of polymer formation depends on the concentration of nuclei: rare, energetically unfavorable oligomers of the polymerizing subunits. Although a biochemically correct kinetic description of MT initiation does not yet exist, we explored the consequences of our observations using a simple nucleation-elongation kinetic model (see *Methods*) that captures essential features of polymer initiation kinetics. To account for the destabilization of early intermediates that we predict result from the lattice model, we lowered the efficiency of the early "nucleation" steps (see Fig. 5*c* and *Methods*). The model predicts that dramatic changes in assembly behavior result from quite modest changes in apparent affinity. For example, a nucleus of size 4 and a straightening penalty $\Delta G_{straight}$ of as little 1.6 *kT* (≈1 kcal/mol) results in a ≈10-fold increase in the time required to reach 10% polymerized (Fig. 5*d*, red and black curves). The extreme sensitivity to nucleation means that even a modest straightening cost should significantly decrease the rate of assembly (Fig. 5*d*). Furthermore, the open lattice structure of the MT suggests that multiple nucleation intermediates will require this "double straightening" and therefore that the associated energetic cost will be incurred multiple times (e.g., Fig. 5 *b* and *c*, reactions with red arrows), producing a dramatic multiplicative effect as the number of steps increase (Fig. 5*e*).

By assuming that $\alpha\beta$-tubulin adopts only the fully curved or the fully straight conformation, we chose the simplest possible

model to explore the kinetic implications of assembly-dependent conformational change. Our demonstration that the conformation of unpolymerized $\alpha\beta$-tubulin:GTP:Mg^{2+} is curved, along with EM or AFM results showing assembly/disassembly intermediates with partial curvature (5, 8, 9, 34), support the idea that straightening occurs incrementally in response to multiple lateral associations (Fig. S5). In general terms, progressive straightening means that the wider the assembly, the more the curved heterodimer initiating a new lateral layer must straighten. The energetic cost of straightening could therefore manifest itself differently for intermediates of different width. Some partial straightening could potentially occur in response to longitudinal self-association, but the fact that partially curved $\alpha\beta$-tubulin assemblies nearly always have at least two protofilaments has made this difficult to determine unambiguously. We have focused on the role of lateral assembly because full straightening is typically only observed after tubulin assemblies are multiple protofilaments wide. A full understanding of the allosteric mechanisms at work in $\alpha\beta$-tubulin assembly that can integrate these concepts into a quantitative understanding of MT assembly dynamics represents a major challenge for the future.

The general requirement that subunits change conformation for self-assembly selectively exaggerates the difficulty of polymer initiation and represents an unanticipated force that should reduce the likelihood of spontaneous nucleation by opposing lateral association. This additional barrier to polymer formation may help explain why MT initiation *in vivo* is especially dependent on a specific nucleator like γ-TuRC (35) that provides MT-like longitudinal stabilization necessary to drive the otherwise unfavorable straightening of $\alpha\beta$-tubulin (Fig. S6). It also helps rationalize the remarkably low nucleation efficiency of smaller γ-tubulin assemblies like the γ-tubulin small complex (36), because these smaller assemblies can only overcome a small number of the necessary lateral additions required for MT formation. Additionally, this new view of MT assembly predicts that, although the γ-phosphate of GTP provides the driving force for assembly via lattice contacts, it is the spring-like conformational strain within $\alpha\beta$-tubulin that determines the energy stored in the metastable MT lattice that is released upon catastrophe. Assembly-dependent conformational change effectively means that polymer formation and polymer disassembly are subject to different energetic constraints. This uncoupling of assembly and disassembly is likely important for MT dynamics *in vivo*.

Methods

Expression, Purification, and Crystallization of γ-Tubulin. Protein expression, purification, and crystallization was performed as reported ref. 10 with minor changes.

Structure Determination. Diffraction data were collected at beamline 8.2.1 (HHMI) at the Advanced Light Source (Berkeley, CA). Data processing and reduction were carried out with HKL2000 (37). Molecular replacement searches and refinement were carried out with phaser (38) and model building was performed with O (39). Initial phases were determined by molecular replacement using a γ-tubulin search model (PDB 1Z5V, ref. 10) with all sidechains truncated to alanine and all cofactors (GTPγS, Mg^{2+}, colchicine, and waters) removed. A conservative approach, along with the improved resolution compared with previous tubulin structures, allowed us to identify a register shift error in H12, the C-terminal helix of the protein (Fig. S1). Figures were made with PyMOL (40).

Allocolchicine Binding. Allocolchicine was prepared by Margot Paulick (U.C. Berkeley) following established methods (23). Solutions of 4 μM $\alpha\beta$-tubulin containing 0, 0.65, 1.3, 2.6, 5.2, 7.8, 11.7, 15.6, 23.4, or 31.2 μM allocolchicine were prepared and equilibrated at 20°C for 2 h before measurement. For each sample, emission spectra were collected between 380 and 420 nm using excitation at 315 nm. The affinity of $\alpha\beta$-tubulin:GTP and $\alpha\beta$-tubulin:GDP for allocolchicine was determined by fitting the normalized fluorescence at 400 nm to the following equation:

$$\text{saturation} = \{(K_d + [\text{ALLO}] + [\alpha\beta]) - \sqrt{(K_d + [\text{ALLO}] + [\alpha\beta])^2 - 4 \times [\text{ALLO}] \times [\alpha\beta]}\} /(2 \times [\alpha\beta]),$$

where K_d represents the dissociation constant for allocolchicine binding, and [ALLO] and $[\alpha\beta]$ denote the total allocolchicine and $\alpha\beta$-tubulin concentrations, respectively. See *SI Methods* for more details.

Small-Angle X-Ray Scattering. Sample preparation, data collection, and the models used for calculations are described in SI Methods. Pair distribution functions were computed by using GNOM (41) from data such that $0 < Q < 0.25$, choosing D_{max} so that the curves tail smoothly to zero probability (95 Å for 1JFF, 1SA0, and the γ-tubulin based curved model; 101 and 103 Å for GTP and GDP data, respectively). Radii of gyration determined from these calculated distributions are 29.6 Å, 30.5 Å, and 31.4 Å for straight (1JFF), curved (1SA0), and model curved conformations, respectively, and 33.0 ± 0.11 Å and 32.7 ± 0.15 Å for experimental GTP- and GDP-bound $\alpha\beta$-tubulin, respectively. The trimmed straight (1JFF), curved (1SA0), and more complete γ-tubulin based curved $\alpha\beta$-tubulin models were fit to the experimental GTP $\alpha\beta$-tubulin SAXS data using CRYSOL (16).

Kinetic Simulations. Nucleation-elongation kinetic models were constructed to explore the potential consequences of assembly-dependent conformational exchange. We used a generic model that ignores the structural details of oligomer organization because the sequence of intermediates leading to microtubule assembly is not known. Having assumed a bimolecular on rate constant of 1×10^6 $M^{-1}s^{-1}$ and subunit concentrations in the 10 μM range, we chose dissociation rate constants such that subunit addition was relatively high affinity during elongation (k_r^{Elon} such that $K_d^{Elon} = 1$ μM) but significantly lower affinity during nucleation (K_r^{Nucl} such that $K_d^{Nucl} = 1$ mM). These parameters capture the essence of nucleation-elongation behavior, and the conclusions we draw are valid over a broad range of parameters. The species at which subunit addition becomes energetically favorable is called the nucleus. Kinetic equations corresponding to a model with a nucleus consisting of N subunits are:

$$\alpha\beta + \alpha\beta \underset{k_r^{Nucl}}{\overset{k_f}{\rightleftarrows}} (\alpha\beta)_2$$

$$(\alpha\beta)_{N-1} + \alpha\beta \underset{k_r^{Nucl}}{\overset{k_f}{\rightleftarrows}} (\alpha\beta)_N$$

$$(\alpha\beta)_N + \alpha\beta \overset{k_f}{\rightarrow} \text{MT}$$

$$\text{MT} + \alpha\beta \underset{k_r^{Elon}}{\overset{k_f}{\rightleftarrows}} \text{MT}$$

where the $(\alpha\beta)_i$ represent subcritical intermediates, MT represents the microtubule polymer, k_f is the bimolecular on-rate constant (assumed to be 1×10^6 $M^{-1}s^{-1}$), and K_r^{Nucl} and k_r^{Elon} are the reverse rate constants for nucleation and elongation, respectively, calculated so as to give the dissociation constants assumed above. As in othe r polymerization models, to avoid wholesale destruction of polymers the reverse rate constant for initial polymer formation was set to 0. Assembly kinetics were simulated in Berkeley Madonna (www.berkeleymadonna.com) assuming a monomer concentration of 10 μM, and the assembly-dependent conformational change was modeled as a decrease in the affinity of nucleation steps (increase in K_r^{Nucl} by a factor of $\exp(\Delta G_{straight}/kT)$, where $\Delta G_{straight}$ denotes the estimated energetic cost for conformational change. Fractional assembly was calculated from $([\alpha\beta]_i - [\alpha\beta]_t)/([\alpha\beta]_i - K_d^{Elon})$, where $[\alpha\beta]_i$ and $[\alpha\beta]_t$ respectively denote the initial and time-dependent concentrations of unassembled $\alpha\beta$-tubulin, and K_d^{Elon} denotes the dissociation constant for elongation. To compare models with different number of intermediates, the time scale of the unpenalized run from each model was rescaled such that 10% assembly occurred at $t = 10$. Initial rates of assembly were calculated from $1/T_{10\%}$, where $T_{10\%}$ denotes the time taken to reach 10% assembly.

ACKNOWLEDGMENTS. We thank Margot Paulick (University of California, Berkeley) for synthesizing allocolchicine and Dan Southworth, Michelle Moritz, and Brian Kelch for helpful comments. We thank the beamline SAXS support staff: Greg Hura (ALS 12.3.1), David Gore, Liang Guo, and Mark Vukonich (APS BIO-CAT), and Hiro Tsuruta (SSRL 4–2). This work was supported by National Institutes of Health Grant GM31627 and the Howard Hughes Medical Institute. L.M.R. was a Paul Sigler/Agouron Institute fellow of the Helen Hay Whitney Foundation.

1. Desai A, Mitchison TJ (1997) Microtubule polymerization dynamics. *Annu Rev Cell Dev Biol* 13:83–117.
2. Lowe J, *et al.* (2001) Refined structure of alpha beta-tubulin at 3.5 Å resolution. *J Mol Biol* 313:1045–1057.
3. Ravelli RB, *et al.* (2004) Insight into tubulin regulation from a complex with colchicine and a stathmin-like domain. *Nature* 428:198–202.
4. Nogales E, Wang HW (2006) Structural mechanisms underlying nucleotide-dependent self-assembly of tubulin and its relatives. *Curr Opin Struct Biol* 16:221–229.
5. Wang HW, Nogales E (2005) Nucleotide-dependent bending flexibility of tubulin regulates microtubule assembly. *Nature* 435:911–915.
6. Buey RM, Diaz JF, Andreu JM (2006) The nucleotide switch of tubulin and microtubule assembly: A polymerization-driven structural change. *Biochemistry* 45:5933–5938.
7. Mandelkow EM, Mandelkow E, Milligan RA (1991) Microtubule dynamics and microtubule caps: a time-resolved cryo-electron microscopy study. *J Cell Biol* 114:977–991.
8. Müller-Reichert T, Chrétien D, Severin F, Hyman AA (1998) Structural changes at microtubule ends accompanying GTP hydrolysis: Information from a slowly hydrolyzable analogue of GTP, guanylyl (α,β)methylenediphosphonate. *Proc Natl Acad Sci USA* 95:3661–3666.
9. Chretien D, Fuller SD, Karsenti E (1995) Structure of growing microtubule ends: two-dimensional sheets close into tubes at variable rates. *J Cell Biol* 129:1311–1328.
10. Aldaz H, *et al.* (2005) Insights into microtubule nucleation from the crystal structure of human gamma-tubulin. *Nature* 435:523–527.
11. Gigant B, *et al.* (2005) *Structural basis for the regulation of tubulin by vinblastine Nature* 435:519–522.
12. Schlieper D, *et al.* (2005) Structure of bacterial tubulin BtubA/B: Evidence for horizontal gene transfer. *Proc Natl Acad Sci USA* 102:9170–9175.
13. Oliva MA, Trambaiolo D, Lowe J (2007) Structural insights into the conformational variability of FtsZ. *J Mol Biol* 373:1229–1242.
14. Lowe J, Amos LJ (1998) Crystal structure of the bacterial cell-division protein FtsZ. *Nature* 391:203–206.
15. Oliva MA, Cordell SC, Lowe J (2004) Structural insights into FtsZ protofilament formation. *Nat Struct Mol Biol* 11:1243–1250.
16. Svergun D, Barberato C, Koch MHJ (1995) CRYSOL: A program to evaluate x-ray solution scattering of biological macromolecules from atomic coordinates. *J Appl Crystallogr* 28:768–773.
17. Shearwin KE, Timasheff SN (1994) Effect of colchicine analogues on the dissociation of alpha beta tubulin into subunits: The locus of colchicine binding. *Biochemistry* 33:894–901.
18. Manuel Andreu J, *et al.* (1989) *A* synchrotron X-ray scattering characterization of purified tubulin and of its expansion induced by mild detergent binding. *Biochemistry* 28:4036–4040.
19. Sontag CA, Staley JT, Erickson HP (2005) In vitro assembly and GTP hydrolysis by bacterial tubulins BtubA and BtubB. *J Cell Biol* 169:233–238.
20. Oliva MA, *et al.* (2003) Assembly of archaeal cell division protein FtsZ and a GTPase-inactive mutant into double-stranded filaments. *J Biol Chem* 278:33562–33570.
21. Kull FJ, Fletterick RJ (1998) Is the tubulin/FtsZ fold related to the G-protein fold? *Trends Cell Biol* 8:306–307.
22. Nogales E, *et al.* (1998) Tubulin and FtsZ form a distinct family of GTPases. *Nat Struct Biol* 5:451–458.
23. Hastie, S.B., (1989) Spectroscopic and kinetic features of allocolchicine binding to tubulin. *Biochemistry* 28:7753–7760.
24. Medrano FJ, *et al.* (1989) Roles of colchicine rings B and C in the binding process to tubulin. *Biochemistry* 28:5589–5599.
25. Shearwin KE, Perez-Ramirez B, Timasheff SN (1994) Linkages between the dissociation of alpha-beta tubulin into subunits and ligand-binding: The ground-state of tubulin is the Gdp conformation. *Biochemistry* 33:885–893.
26. Perez-Ramirez B, Shearwin KE, Timasheff SN (1994) The colchicine-induced GTPase activity of tubulin: state of the product: Activation by microtubule-promoting cosolvents. *Biochemistry* 33:6253–6261.
27. Amayed P, Carlier MF, Pantaloni D (2000) Stathmin slows down guanosine diphosphate dissociation from tubulin in a phosphorylation-controlled fashion. *Biochemistry* 39:12295–12302.
28. Melki R, Carlier MF, Pantaloni D (1988) Oscillations in microtubule polymerization: the rate of GTP regeneration on tubulin controls the period. *EMBO J* 7:2653–2659.
29. Davies JM, *et al.* (2005) Conformational changes of p97 during nucleotide hydrolysis determined by small-angle X-Ray scattering. *Structure* 13:183–195.
30. Koch MH, Vachette P, Svergun DI (2003) Small-angle scattering: A view on the properties, structures and structural changes of biological macromolecules in solution. *Q Rev Biophys* 36:147–227.
31. Nagar B, *et al.* (2006) Organization of the SH3-SH2 unit in active and inactive forms of the c-Abl tyrosine kinase. *Mol Cell* 21:787–798.
32. Walker RA, *et al.* (1988) Dynamic instability of individual microtubules analyzed by video light microscopy: Rate constants and transition frequencies. *J Cell Biol* 107:1437–1448.
33. Ferrone, F (1999) Analysis of protein aggregation kinetics. *Methods Enzymol* 309:256–274.
34. Elie-Caille C, *et al.* (2007) Straight GDP-tubulin protofilaments form in the presence of taxol. *Curr Biol* 17:1765–1770.
35. Moritz M, *et al.* (2000) Structure of the gamma-tubulin ring complex: a template for microtubule nucleation. *Nat Cell Biol* 2:365–370.
36. Oegema K, *et al.* (1999) Characterization of two related Drosophila gamma-tubulin complexes that differ in their ability to nucleate microtubules. *J Cell Biol* 144:721–733.
37. Minor W, Cymborowski M, Otwinowski Z (2002) Automatic system for crystallographic data collection and analysis. *Acta Physica Polonica A* 101:613–619.
38. Storoni LC, McCoy AJ, Read RJ (2004) Likelihood-enhanced fast rotation functions. *Acta Crystallogr D* 60:432–438.
39. Jones TA, *et al.* (1991) Improved methods for building protein models in electron density maps and the location of errors in these models. *Acta Crystallogr A* 47:110–119.
40. DeLano WL (2002) *The PyMol Molecular Graphics System* (Delano Scientific, San Carlos, CA), www.pymol.org.
41. Svergun DI (1992) Determination of the regularization parameter in indirect-transform methods using perceptual criteria. *J Appl Crystallogr* 25:495–503.